Highly Resolved Measurements of a Developing Strong Collisional Plasma Shock

Hans G. Rinderknecht,[1,*] H.-S. Park,[1] J. S. Ross,[1] P. A. Amendt,[1] D. P. Higginson,[1] S. C. Wilks,[1] D. Haberberger,[2] J. Katz,[2] D. H. Froula,[2] N. M. Hoffman,[3] G. Kagan,[3] B. D. Keenan,[3] and E. L. Vold[3]
[1]*Lawrence Livermore National Laboratory, Livermore, California 94550, USA*
[2]*Laboratory for Laser Energetics, Rochester, New York 14623, USA*
[3]*Los Alamos National Laboratory, Los Alamos, New Mexico 87545, USA*

(Received 30 November 2017; revised manuscript received 26 January 2018; published 2 March 2018)

The structure of a strong collisional shock front forming in a plasma is directly probed for the first time in laser-driven gas-jet experiments. Thomson scattering of a 526.5 nm probe beam was used to diagnose temperature and ion velocity distribution in a strong shock ($M \sim 11$) propagating through a low-density ($\rho \sim 0.01$ mg/cc) plasma composed of hydrogen. A forward-streaming population of ions traveling in excess of the shock velocity was observed to heat and slow down on an unmoving, unshocked population of cold protons, until ultimately the populations merge and begin to thermalize. Instabilities are observed during the merging, indicating a uniquely plasma-phase process in shock front formation.

DOI: 10.1103/PhysRevLett.120.095001

Shocks are ubiquitous phenomena in high-energy-density (HED) plasmas, and are important both in astrophysics and laser-plasma experiments such as inertial confinement fusion (ICF). At large distances relative to the shock front width Δx, the shocked plasma state may be calculated from the unshocked (upstream) density and pressure and the shocked (downstream) fluid velocity [1]. However, conditions near the shock front are often important: for example, the radially converging shock in an ICF implosion inevitably violates this condition when reaching a radius $R \leq \Delta x$. Moreover, hydrodynamic treatments [2] are insufficient to calculate the structure of a strong shock front with Mach number $M \gtrsim 1.5$, defined as the ratio of the shock velocity to the upstream sound speed (u_{sh}/c_s) [3].

In strong collisional plasma shocks, kinetic ion distributions at the discontinuity extend to tens of times the ion thermal mean free path in the shocked plasma (λ_{ii}) [4,5]. Strong collisional [6–8], collisionless [9–16], and magnetized shocks [17] have been studied in laboratory plasmas, but despite substantial theoretical effort, few measurements of collisional shock-front structure—profiles of temperature, density, and velocity distribution within the front—have been performed [18]. Profiles of electric field were recently measured in strong plasma shocks [19]; however, the extremely small length and time scales of collisions in most experimental plasmas make measurements of shock structure particularly difficult.

This Letter presents the first measurements of strong, collisional plasma shock-front structure in the formation stage. In experiments using the OMEGA laser [20], strong shocks ($M \sim 11$) were driven into a volume of hydrogen gas, injected by a gas-jet system prior to the laser firing. The volume was interrogated using a 526.5 nm (2ω) probe beam impulse [21]. The Thomson-scattered light from this probe was imaged and used to infer spatially resolved temperature, density, and flow velocity within the shock front [22]. These experiments demonstrate for the first time ion velocity separation within a plasma shock.

In general, strong collisional plasma shock formation can be understood as follows. Electron conduction creates a preheat layer with increased electron temperature ahead of the density jump. The thickness of this layer is predicted to be $\sim\lambda_{ii}\sqrt{m_i/m_e}$, set by the difference in electron and ion thermal velocities [23]. The increased temperature reduces stopping power in the preheat region, allowing the most energetic shocked ions with the largest mean free paths [$\lambda(\epsilon) = (\epsilon/T_i)^2\lambda_{ii}$] to stream forward. The balance of ion stopping power, electron-ion thermalization, ion-ion drag, and collisional heating establishes the shock-front structure.

The experimental layout is shown in Fig. 1. A gas-jet nozzle (5 mm diameter) injects a Mach-3 cone of hydrogen gas (atomic density $\sim 5 \times 10^{18}$ cm^{-3}) into the target chamber. Ten laser beams containing 2.4 kJ in a 1 mm diameter spot drive a 1 μm-thick silicon nitride ablator foil positioned near the gas jet, with a maximum intensity of 500 TW/cm^2. The driven foil explodes, launching a strong shock into the gas. After a delay of 4.1 ns, a 2ω laser impulse containing 40 J in 100 ps is injected along the foil axis to probe the state of the plasma by Thomson scattering. The dimensionless scattering parameter $\alpha \equiv 1/k\lambda_{\mathrm{Debye}} > 1$, so the spectrum is dominated by collective scattering [24]. The scattered spectrum was recorded using both narrow- and wide-band spectrometers, for the ion acoustic wave (IAW) and electron plasma wave (EPW) features, respectively. The IAW feature encodes information about the flow velocity, density, and temperature of ion populations, whereas the EPW feature encodes the electron density and temperature [25]. The spectra were imaged along one

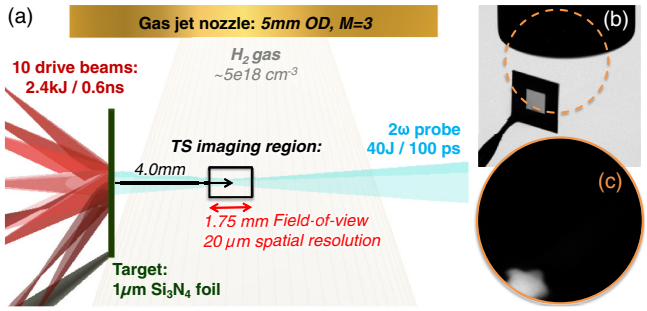

FIG. 1. (a) Experimental design to probe plasma shock front structure. Laser beams drive a Si_3N_4 foil, launching a strong shock into a H_2 gas jet. Thomson-scattered light from a 2ω beam aligned with the foil axis is imaged in a 1.75 mm region, 4.0 mm from the foil. (b) View of the target foil aligned near the gas-jet nozzle. (c) Pinhole camera image showing x rays ($h\nu > 1.5$ keV) from the foil.

spatial dimension, recording a 1.75 mm field of view along the probe axis with 20 μm resolution [26]. The scattering k vector was oriented ~60° from the direction of flow. In this geometry, plasma flowing away from the ablator produces a blueshift in the scattered light. X-ray pinhole cameras recorded self-emission from the irradiated targets, confirming the target survives exposure to the gas jet [Fig. 1(c)]; x rays from the target preheat the hydrogen gas ahead of the shock.

Figures 2(a)–2(b) show Thomson scattering images of the shocked plasma. These images record the formation of the shock front, and notably resolve the ion velocity-space evolution within the shock front. To the best of our knowledge, these data represent the first record of velocity structure within a strong collisional plasma shock. A qualitative discussion reveals many interesting details of strong plasma shock formation: ions streaming in excess of the shock velocity (dashed purple line) first interact with the cold proton gas (two peaks symmetric around the initial wavelength, indicating negligible flow velocity). This interaction heats the unshocked ions (green arrows, broadening of unshocked feature) and electrons (broadening of electron feature). The streaming and unstreaming populations merge at a flow velocity of ~750 μm/ns, with rapid changes in the IAW feature.

This qualitative picture is supported by quantitative analysis, performed by forward fitting a scattered-spectrum model to the data [24]. Figure 2(c) shows fits to the EPW data. Fitting uncertainty was calculated using a reduced chi-squared method. These data show the characteristic shock features [5]: an electron preheat layer is observed in which the temperature increases from 220 to 350 eV, followed by an increase in density from 0.5 to 3.1×10^{19} cm^{-3} and temperature to 480 eV. Moreover, the IAW spectra in the electron preheat region verify the primary prediction of the kinetic theory of strong shocks: an energetic, forward-streaming ion population extends throughout the electron preheat layer.

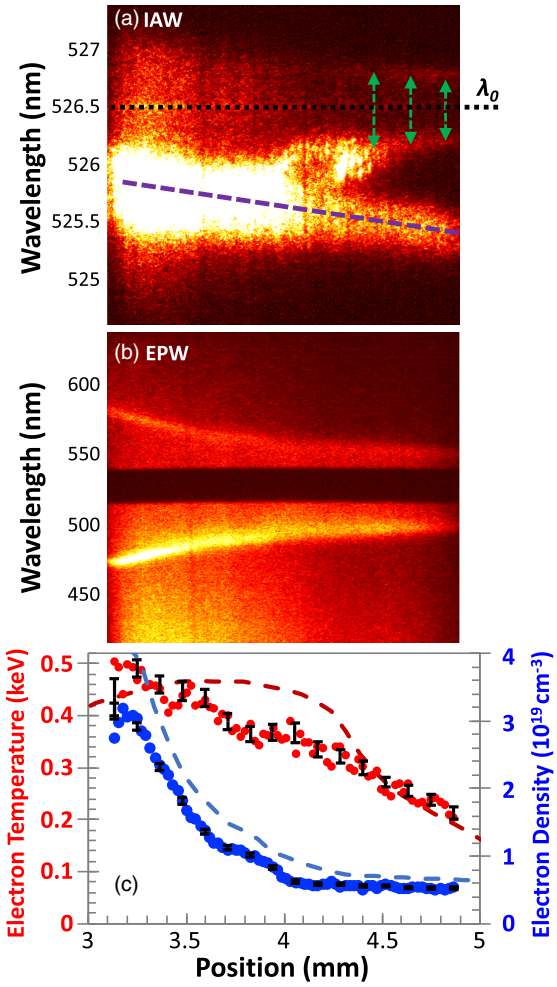

FIG. 2. Thomson scattering images of the shocked plasma: (a) IAW and (b) EPW features recorded 4.1 ns after the laser drive. Spatial dimension is horizontal, with the shock propagating to the right. The IAW image captures the shock transition, showing a forward-streaming population (purple) slowing on and heating a cold, still population (green). (c) Fits to the EPW spectra provide electron temperature (red) and density (blue), showing the preheat region followed by the density jump. Error bars indicate typical fitting uncertainty. Trends from PIC simulations (dashed) capture the density jump position and temperature magnitude.

Using these measurements, plasma parameters of interest are calculated in both the preheat and shock region (Table I). The thermal mean free path for hydrogen ions in the shocked plasma is estimated to be 170 ± 20 μm: over 10^3 times the estimated Debye length, confirming the assumption of quasineutrality for this plasma.

Kinetic theory [4,27] and simulations [5] suggest that the width of the electron preheat region should be $\Delta x \approx \lambda_{ii}\sqrt{m_i/m_e} \approx 8$ mm. This prediction exceeds the instrument field of view, and indeed the distance from the foil to the imaged area. While the images do not record the entire electron preheat region, linear extrapolation implies the region extends ~1 mm beyond the imaged area, indicating

TABLE I. Plasma parameters in shock and preheat regions.

Parameter	Shock	Preheat
Sound speed, c_s (μm/ns)	285	90
Debye length, λ_{De} (μm)	0.019	0.016
Plasma frequency, ω_{pe} (ns^{-1})	3×10^5	1.3×10^5
Ion skin depth, c/ω_{pi} (μm)	47	99
Hydrogen thermal mean free path, λ_H (μm)	170	10
Flow velocity, v (μm/ns)	750	0

a shock width of 3 mm: approximately one-third of the predicted scaling. The reason for this discrepancy is likely that the shock has not yet fully formed. Vidal *et al.* [5] show that a shock requires spatial separation of approximately $2\Delta x$ from the pusher to reach steady state, before which the shock is in a transient formation stage, asymptotically approaching its final width from below. Given the velocity difference between the front and the shocked fluid $[(u_{sh} - v_1) = u_{sh}(\gamma - 1)/(\gamma + 1) \approx u_{sh}/4]$, the time required to reach a steady state is estimated as $t_S \approx 8\Delta x/u_{sh}$. Taking $u_{sh} = x_{meas}/t_{meas} \sim 1000$ μm/ns, the steady-state time is $t_S \approx 24$ ns, 6 times longer than the sample time. This estimate corroborates our observation of a narrow shock compared to the analytical prediction.

A Thomson scattering model with multiple ion populations was forward-fit to interpret the IAW data. Figure 3 shows representative fits in the preheat and shock regions, and the results of these fits. The model includes the effects of finite optics [28,29]. In the preheat (4.5–5 mm) and density-jump (3–4 mm) regions, the hydrogen distribution is well represented as the sum of two flowing Maxwellians: a hot population streaming forward at ~1000 μm/ns and a cold population not flowing with respect to the lab frame. Additionally, a small population of forward-streaming Si and N ions is required to match the narrow, blueshifted peak observed throughout the imaged region. Accurate fits are obtained assuming these ions share the same composition as the fully ionized target foil [30]. Given the relatively high density of the Si_3N_4 pusher, some pusher ions are predicted to stream into the low-density hydrogen plasma while the shock forms [31]. The velocity of the Si_3N_4 ions is similar to the free-streaming velocity [Fig. 3(e)].

Within the preheat region, the calculated sound-speed of the background protons ($T_i = 50$ eV $\Rightarrow c_s = 90$ μm/ns), confirms a strong shock ($M \approx 11$). The hot streaming population constitutes approximately 20% of the protons. These are substantially hotter (~3 keV) and faster (~1200 μm/ns) than the shocked plasma, and are also hotter than the electrons. The high fraction and temperature of the streaming population is consistent with a forming shock front: in steady state, $T_e > T_i$ and $f_{hot} \sim 10\%$ in the preheat region, whereas in a forming shock the streaming ions are hotter and more numerous [5].

At the beginning of the density jump, the data show acceleration and heating of the cold protons as the hot

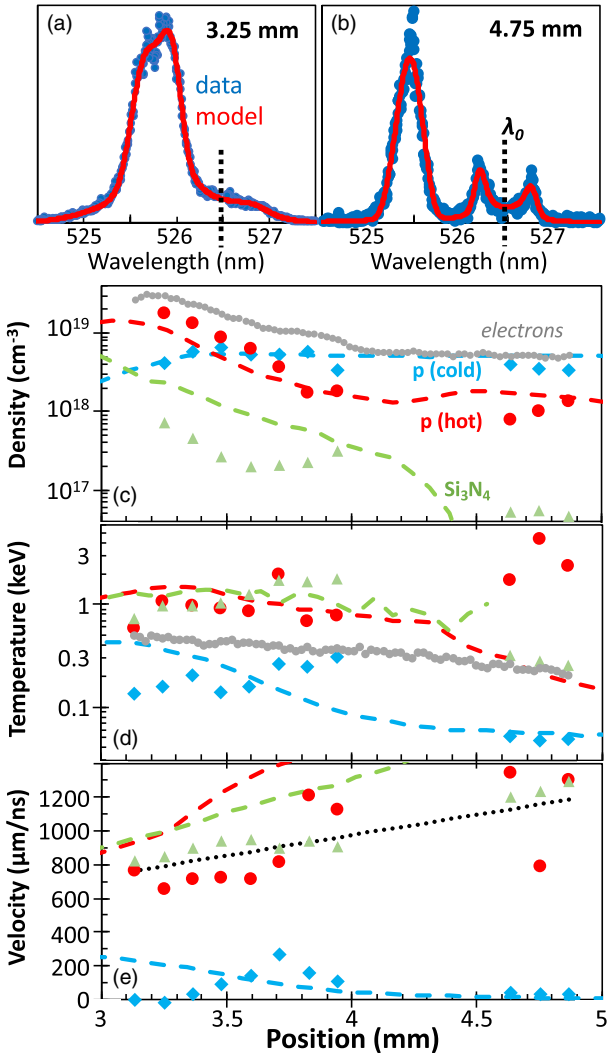

FIG. 3. (a), (b) Example lineouts and fits to IAW spectra in the shock and preheat region. (c)–(e) Density, temperature, and velocity from fits to the IAW spectra. Data were accurately matched using three ion populations: cold background hydrogen (blue diamonds), hot streaming hydrogen (red circles), and streaming ablator ions (green triangles). Electron density and temperature (grey) and free-streaming velocity (black dotted) are included for reference. Results of PIC simulations (dashed) capture trends in proton density and temperature.

population slows. The hot population density exceeds the cold population near 3.5 mm, and continues to grow toward the foil, reaching an asymptotic temperature (~1 keV) and velocity (~700 μm/ns). In contrast, the cold population density drops as the ion shock forms. Behind the density jump, the remaining cold population (~20%) has increased in temperature from the preshock value by 4×.

Immediately ahead of the density jump (4.0–4.5 mm), the scattered light spectrum varies rapidly, and accurate fits of the three-population model could not be found. In particular, near $\lambda = 526$ nm a flashing pattern is observed: four peaks separated by 40 ± 10 μm, with increasing

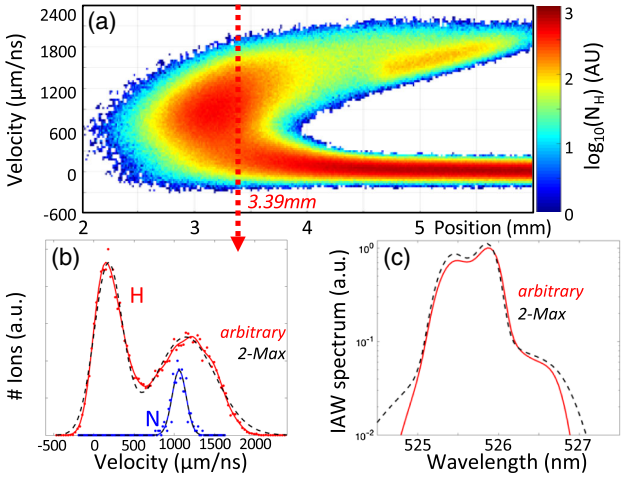

FIG. 4. Results from PIC simulation: (a) Hydrogen velocity-position phase space at the experimental sample time. (b) Hydrogen (red) and nitrogen distributions (blue), 3.39 mm from the foil, with arbitrary (red solid) and 2-Maxwellian (black dashed) fits to the H and Maxwellian fit (blue solid) to N. (c) Simulated Thomson-scattering spectrum at 3.39 mm using arbitrary and thermal fits.

brightness toward the density jump. Vidal *et al.* [5] report that electrostatic instability growth is possible within a Mach 5 shock for times $0.15 < t/t_S < 0.43$. The present experiment falls within this range, suggesting the flashing is a signature of instability growth. The fastest-growing wavelength of the ion-ion two-stream instability in this plasma is on the order of a few microns, smaller than the instrument resolution and thus not directly observable [32]. However, the growth rate of such modes is rapid ($\sim\omega_{pi} > 300$ ns^{-1}). The intensity of the feature grows exponentially as $\sim\exp(x[20\ \mu\text{m}^{-1}])$. Comparing to the shock velocity, this implies a growth rate on the order of 10^4 ns^{-1}.

For comparison to the data, a simulation was performed using the particle-in-cell (PIC) code LSP [33]. This simulation is similar to Ref. [34], with fully-implicit kinetic ions undergoing binary collisions, and fluid electrons [35]. A Si_3N_4 plasma pushes a 50 eV, 5×10^{18} cm^{-3} hydrogen plasma. The initial conditions for the Si_3N_4 were taken from a planar 1D simulation using the radiation-hydrodynamic code HYADES [36] at 1.0 ns. The ion distributions produced 4.1 ns after the initial laser drive were fit using a bi-Maxwellian model for the hydrogen and a thermal model for the silicon and nitrogen, as shown in Figs. 4(a)–4(b); the results are shown as dashed lines in Figs. 2 and 3. The model captures many features observed in the data, including the electron density and temperature [Fig. 2(c)], the relative trends of density in the hot- and cold-proton populations [Fig. 3(c)], and the heating and velocity of the cold population [Figs. 3(d), 3(e)]. However, the model fails to capture the density of the Si_3N_4 ions, and the velocities of the forward-streaming ions (which are consistent with the free-streaming velocity). It is notable that, while the simulated electron density jump leads the data by 0.1–0.2 mm, the increase in density of the hot protons lags behind the data by 0.2 mm. This discrepancy indicates that the code is not accurately capturing the dynamics of shock stagnation, which is more rapid in the experiment.

The simulations confirm bi-Maxwellian fits are a reasonable approximation. However, the Thomson scattering form factor is in principle sensitive to nonthermal distributions. To assess whether this affects the data, a nonthermal model was developed, composed of evenly spaced Maxwellians with amplitudes fit to the simulated hydrogen distribution. Figures 4(b)–4(c) show a best fit of this arbitrary model (using 20 peaks) and its effect on the Thomson-scattered spectrum. This model performed better than the 2-Maxwellian fit primarily within the density jump (3.2–3.6 mm in the simulation, 3.4–3.8 mm in the data). In this region, the 2-Maxwellian fit overestimates the tail of the distribution; with the higher-resolution model, the edges of the scattered light spectrum fall off more rapidly. Notably, the 2-Maxwellian model is highly accurate ahead of the density jump (3.7–4.2 mm in the simulation, 3.9–4.4 mm in the data), despite the fact that accurate fits to the data could not be found. This discrepancy, in combination with the more rapid increase in the hot proton fraction in the data, suggests that instability in the experiment stagnates the ion flows more efficiently than the simulation predicts.

In conclusion, the structure of a strong ($M \approx 11$) collisional plasma shock front has been measured for the first time using optical Thomson scattering. Three-population fits to the data demonstrate the kinetic structure of strong-shock formation: a hot population of ions streaming through the cold background in the preheat region, heating and drag of the cold background, and rapid increase of the hot population within the density jump. The relatively short preheat region ($\sim\lambda_H\sqrt{m_i/m_e}/3$) observed in data and simulation confirms that strong shocks approach their steady-state width from below. Kinetic simulations reproduce the density, electron temperature, and proton population trends observed in the data, but do not capture the flashing observed prior to the density jump, and under predict the rate of shock stagnation, suggesting two-stream instability plays a role in the shock formation. The data provide an unprecedented level of detail in examining ion collisional processes in high-energy-density plasmas. In future studies, the ion mean free path will be controlled to obtain a scaling of shock width and formation time with Mach number. Simultaneous measurement of electric field structures [19] will further improve understanding of these phenomena. The relatively long time (~20 ns) and length scales (~cm) needed for full shock formation may require laser energy on the scale of the National Ignition Facility [37], where an Optical Thomson Scattering (OTS) diagnostic is now available [38,39]. This research program offers a new challenge to high-fidelity physics codes, for

improved accuracy in modeling plasmas of interest to ICF and laboratory astrophysics.

The authors would like to acknowledge valuable conversations with Luis Chacon, Andrei Simakov, and Will Taitano. This work was performed under the auspices of the U.S. Department of Energy by LLNL under Contract No. DE-AC52-07NA27344, and supported by the LLNL Laboratory Directed Research and Development Program (LDRD) (17-ERD-060, 18-ERD-047). Laser system time provided by the Laboratory Basic Science (LBS) program at the University of Rochester Laboratory for Laser Energetics.

*rinderknecht1@llnl.gov

[1] W. J. M. Rankine, Phil. Trans. R. Soc. London **160**, 277 (1870).
[2] M. Y. Jaffrin and R. F. Probstein, Phys. Fluids **7**, 1658 (1964).
[3] B. D. Keenan, A. N. Simakov, L. Chacon, and W. T. Taitano, Phys. Rev. E **96**, 053203 (2017).
[4] M. S. Greywall, Phys. Fluids **18**, 1439 (1975).
[5] F. Vidal, J. P. Matte, M. Casanova, and O. Larroche, Phys. Fluids B **5**, 3182 (1993).
[6] R. A. Bosch, R. L. Berger, B. H. Failor, N. D. Delamater, G. Charatis, and R. L. Kauffman, Phys. Fluids B **4**, 979 (1992).
[7] E. C. Merritt, A. L. Moser, S. C. Hsu, J. Loverich, and M. Gilmore, Phys. Rev. Lett. **111**, 085003 (2013).
[8] A. L. Moser and S. C. Hsu, Phys. Plasmas **22**, 055707 (2015).
[9] A. R. Bell, P. Choi, A. E. Dangor, O. Willi, D. A. Bassett, and C. J. Hooker, Phys. Rev. A **38**, 1363 (1988).
[10] R. L. Berger, J. R. Albritton, C. J. Randall, E. A. Williams, W. L. Kruer, A. B. Langdon, and C. J. Hanna, Phys. Fluids B **3**, 3 (1991).
[11] L. Romagnani, S. V. Bulanov, M. Borghesi, P. Audebert, J. C. Gauthier, K. Löwenbrück, A. J. Mackinnon, P. Patel, G. Pretzler, T. Toncian, and O. Willi, Phys. Rev. Lett. **101**, 025004 (2008).
[12] Y. Kuramitsu, Y. Sakawa, T. Morita, C. D. Gregory, J. N. Waugh, S. Dono, H. Aoki, H. Tanji, M. Koenig, N. Woolsey, and H. Takabe, Phys. Rev. Lett. **106**, 175002 (2011).
[13] H.-S. Park, D. D. Ryutov, J. S. Ross, N. L. Kugland, S. H. Glenzer, C. Plechaty, S. M. Pollaine, B. A. Remington, A. Spitkovsky, L. Gargate, G. Gregori, A. Bell, C. Murphy, Y. Sakawa, Y. Kuramitsu, T. Morita, H. Takabe, D. H. Froula, G. Fiksel, F. Miniati*et al.*, High Energy Density Phys. **8**, 38 (2012).
[14] H. Ahmed, M. E. Dieckmann, L. Romagnani, D. Doria, G. Sarri, M. Cherchez, E. Ianni, I. Kourakis, A. L. Giesecke, M. Notley, R. Prasad, K. Quinn, O. Willi, and M. Borghesi, Phys. Rev. Lett. **110**, 205001 (2013).
[15] J. S. Ross, D. P. Higginson, D. Ryutov, F. Fiuza, R. Hatarik, C. M. Huntington, D. H. Kalantar, A. Link, B. B. Pollock, B. A. Remington, H. G. Rinderknecht, G. F. Swadling, D. P. Turnbull, S. Weber, S. Wilks, D. H. Froula, M. J. Rosenberg, T. Morita, Y. Sakawa, H. Takabe*et al.*, Phys. Rev. Lett. **118**, 185003 (2017).
[16] T. Morita, Y. Sakawa, Y. Kuramitsu, S. Dono, H. Aoki, H. Tanji, J. N. Waugh, C. D. Gregory, M. Koenig, N. C. Woolsey, and H. Takabe, Phys. Plasmas **24**, 072701 (2017).
[17] S. V. Lebedev, L. Suttle, G. F. Swadling, M. Bennett, S. N. Bland, G. C. Burdiak, D. Burgess, J. P. Chittenden, A. Ciardi, A. Clemens, P. De Grouchy, G. N. Hall, J. D. Hare, N. Kalmoni, N. Niasse, S. Patankar, L. Sheng, R. A. Smith, F. Suzuki-Vidal, J. Yuan*et al.*, Phys. Plasmas **21**, 056305 (2014).
[18] R. E. Center, Phys. Fluids **10**, 1777 (1967).
[19] R. Hua, H. Sio, S. C. Wilks, F. N. Beg, C. McGuffey, M. Bailly-Grandvaux, G. W. Collins, and Y. Ping, Appl. Phys. Lett. **111**, 034102 (2017).
[20] T. R. Boehly, D. L. Brown, R. S. Craxton, R. L. Keck, J. P. Knauer, J. H. Kelly, T. J. Kessler, S. A. Kumpan, S. J. Loucks, S. A. Letzring, F. J. Marshall, R. L. McCrory, S. F. B. Morse, W. Seka, J. M. Soures, and C. P. Verdon, Opt. Commun. **133**, 495 (1997).
[21] A. J. Mackinnon, S. Shiromizu, G. Antonini, J. Auerbach, K. Haney, D. H. Froula, J. Moody, G. Gregori, C. Constantin, C. Sorce, L. Divol, R. L. Griffith, S. Glenzer, J. Satariano, P. K. Whitman, S. N. Locke, E. L. Miller, R. Huff, K. Thorp, W. Armstrong*et al.*, Rev. Sci. Instrum. **75**, 3906 (2004).
[22] J. Katz, J. S. Ross, C. Sorce, and D. H. Froula, J. Instrum. **8**, C12009 (2013).
[23] Y. B. Zel'dovich and Y. P. Raizer, *Physics of Shock Waves and High-Temperature Hydrodynamic Phenomena*, Dover Books on Physics (Dover Publications, New York, 2002).
[24] *Plasma Scattering of Electromagnetic Radiation*, edited by D. H. Froula, S. H. Glenzer, N. C. Luhmann, and J. Sheffield, 2nd ed. (Academic Press, Boston, 2011).
[25] J. S. Ross, H. S. Park, P. Amendt, L. Divol, N. L. Kugland, W. Rozmus, and S. H. Glenzer, Rev. Sci. Instrum. **83**, 10E323 (2012).
[26] J. S. Ross, D. H. Froula, A. J. Mackinnon, C. Sorce, N. Meezan, S. H. Glenzer, W. Armstrong, R. Bahr, R. Huff, and K. Thorp, Rev. Sci. Instrum. **77**, 10E520 (2006).
[27] M. Casanova, O. Larroche, and J.-P. Matte, Phys. Rev. Lett. **67**, 2143 (1991).
[28] R. K. Follett, J. A. Delettrez, D. H. Edgell, R. J. Henchen, J. Katz, J. F. Myatt, and D. H. Froula, Rev. Sci. Instrum. **87**, 11E401 (2016).
[29] Velocities are assumed to be along the target axis; the $\vec{k} \cdot \vec{V}$ projection is removed from the reported value.
[30] Simulations predict the N/Si ratio is constant (4/3) until the ions slow significantly.
[31] C. Bellei and P. A. Amendt, Phys. Plasmas **24**, 040703 (2017).
[32] J. D. Huba, NRL Plasma Formulary, (online) (Naval Research Laboratory, Washington, D.C. 2006), DOI: 10.21236/ada447173.
[33] D. R. Welch, D. V. Rose, B. V. Oliver, and R. E. Clark, Nucl. Instrum. Methods Phys. Res., Sect. A **464**, 134 (2001).
[34] C. Bellei, H. Rinderknecht, A. Zylstra, M. Rosenberg, H. Sio, C. K. Li, R. Petrasso, S. C. Wilks, and P. A. Amendt, Phys. Plasmas **21**, 056310 (2014).
[35] Flux limiter = 0.2. Simulations with kinetic electrons were highly consistent with the fluid case.
[36] J. T. Larsen and S. M. Lane, J. Quant. Spectrosc. Radiat. Transfer **51**, 179 (1994).

[37] E. I. Moses, Nucl. Fusion **49**, 104022 (2009).
[38] J. S. Ross, P. Datte, L. Divol, J. Galbraith, D. H. Froula, S. H. Glenzer, B. Hatch, J. Katz, J. Kilkenny, O. Landen, A. M. Manuel, W. Molander, D. S. Montgomery, J. D. Moody, G. Swadling, and J. Weaver, Rev. Sci. Instrum. **87**, 11E510 (2016).
[39] J. Galbraith, P. Datte, S. Ross, G. Swadling, S. Manuel, B. Molander, B. Hatch, D. Manha, M. Vitalich, and B. Petre, in *Proceedings Volume 9966, Target Diagnostics Physics and Engineering for Inertial Confinement Fusion V*, edited by J. A. Koch and G. P. Grim (SPIE-International Society for Optical Engineering, Bellingham, WA, 2016), p. 99660E.